ADVANCES IN ATMOSPHERIC SCIENCES, VOL. 24, NO. 4, 2007, 700–711

Estimating Tropical Cyclone Precipitation from Station Observations

REN Fumin*[1,2] (任福民), WANG Yongmei[3] (王咏梅), WANG Xiaoling[2] (王小玲), and LI Weijing[2] (李维京)

[1] *State Key Laboratory of Numerical Modeling for Atmospheric Sciences and Geophysical Fluid Dynamics, Institute of Atmospheric Physics, Chinese Academy of Sciences, Beijing* 100029

[2] *National Climate Center, China Meteorological Administration, Beijing* 100081

[3] *Yuncheng Weather Bureau, Yuncheng* 044000

(Received 22 May 2006; revised 6 September 2006)

ABSTRACT

In this paper, an objective technique for estimating the tropical cyclone (TC) precipitation from station observations is proposed. Based on a comparison between the Original Objective Method (OOM) and the Expert Subjective Method (ESM), the Objective Synoptic Analysis Technique (OSAT) for partitioning TC precipitation was developed by analyzing the western North Pacific (WNP) TC historical track and the daily precipitation datasets. Being an objective way of the ESM, OSAT overcomes the main problems in OOM, by changing two fixed parameters in OOM, the thresholds for the distance of the absolute TC precipitation (D_0) and the TC size (D_1), into variable parameters.

Case verification for OSAT was also carried out by applying CMORPH (Climate Prediction Center MORPHing technique) daily precipitation measurements, which is NOAA's combined satellite precipitation measurement system. This indicates that OSAT is capable of distinguishing simultaneous TC precipitation rain-belts from those associated with different TCs or with middle-latitude weather systems.

Key words: tropical cyclone precipitation, the Original Objective Method, comparison analysis, the Objective Synoptic Analysis Technique

DOI: 10.1007/s00376-007-0700-y

1. Introduction

Many studies have focused on the precipitation that is associated with tropical cyclones (TCs) (Gleason et al., 2000; Phil and Douglas, 2001; Ren et al., 2002; Akira et al., 2005). A remaining critical issue requires an estimation of the TC precipitation from the daily rainfall records, which usually also consists of the influences of other weather systems.

One way to partition TC precipitation is to analyze synoptic "hand-analysis" maps. This method has been used by the Shanghai Typhoon Institute for more than 50 years and is referred to as the Expert Subjective Method (ESM) in this paper. The ESM can provide a valuable reference for weather forecasts, however, it takes a long time to complete and its results are subjective. Therefore, it is necessary to find an effective approach to obtain objective methods for separating TC precipitation. In previous studies, a certain circle with a fixed radius around a TC center was used to define the region for TC precipitation (Phil and Douglas, 2001; Akira et al., 2005) by assuming that the area influenced by any TC in a certain region doesn't change. As we know, TC sizes can vary from several hundreds to more than 1000 kilometers (Elsberry et al., 1987). In this case, a small, fixed circle won't encompass the total precipitation of a large TC. On the contrary, too large of a circle will include precipitation from other weather systems. Therefore, a fixed circle method often incorrectly partition TC precipitation from the total precipitation.

To overcome this weakness, one may think of employing an adaptive circle size, with the radius being set corresponding to the intensity of the TC. The chal-

*Corresponding author: REN Fumin, fmren@163.com

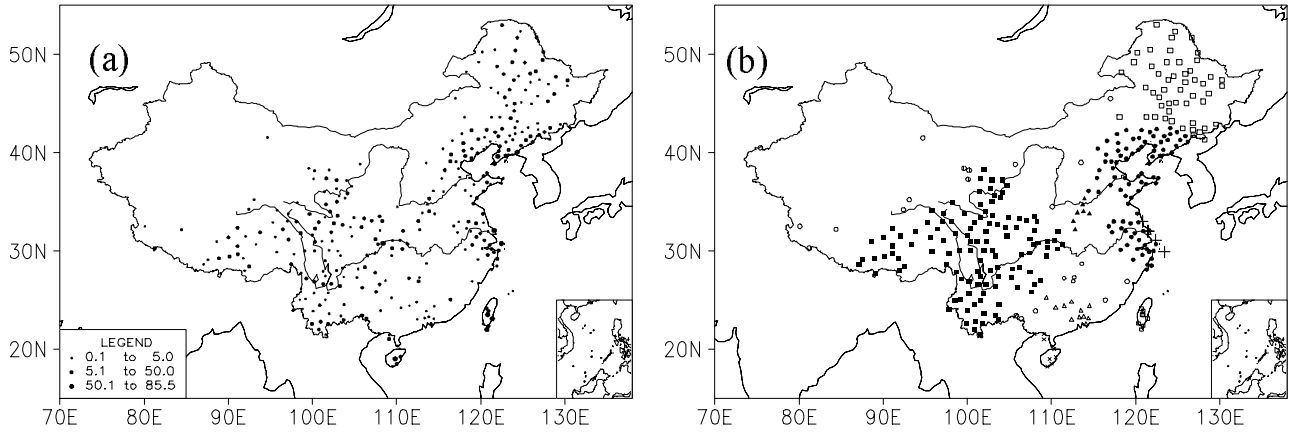

Fig. 1. An example of the partitioning of the TC precipitation. (a) The distribution of the n station daily precipitations (Unit: mm) and (b) the results of the partitioning of the TC precipitation. The "+" denotes the location of the TC center and "•" is used for the TC precipitation, while other symbols refer to other rainbelts or scattered precipitation stations.

lenge with this method is to get reliable TC size information during its lifetime. Nowadays, three different kinds of TC datasets are available: (1) traditional TC position and intensity (minimum central pressure or maximum wind speed, in the western North Pacific with datasets available since 1949), (2) U. S. Air Force aircraft reconnaissance data, and (3) satellite observed datasets. Although the TC size information can be estimated according to different definitions of the TC size, the relationships between the TC size and its intensity are not sufficient for obtaining the necessary information about the TC size from these datasets (Merrill, 1984; Weatherford and Gray, 1988a; Liu and Chan, 1999). Using the average radius of the outer-closed isobar (ROCI) as a measurement of TC size, Merrill (1984) found that in both the western North Pacific and the Atlantic Ocean that the typical TC size varies seasonally and regionally and is only weakly correlated with cyclone intensity. An in-depth analysis of the TC outer wind structure by Weatherford and Gray (1988a,b), based entirely on aircraft reconnaissance data, indicated that the R–15 (the mean radius of the 15 m s^{-1} surface winds around a TC's center, another definition of TC size) and R–25 (the same as R–15 but for 25 m s^{-1}) values were also only weakly correlated with cyclone minimum sea level pressure (MSLP). Using data from the European Remote-Sensing Satellites 1 and 2 (ERS-1 and ERS-2), with the size of a TC being defined as the mean radius at which the relative vorticity decreases to 10^{-5} s^{-1}, a study by Liu and Chan (1999) showed that the mean TC size in the western North Pacific (WNP) also varied seasonally, with larger values observed in late autumn in comparison to midsummer. These results generally indicate that TC size information cannot be directly derived from the TC intensity. For this reason, the adaptive circle method is also questionable.

In addition, several discontinuous rain-belts may exist in a given TC at one time, which are generally asymmetric with respect to the TC center (Elsberry et al., 1987). Thus, simply using a circle around a TC center cannot capture asymmetric TC rain-belts satisfactorily, while the aforementioned subjective method can identify such asymmetric rain-belts. Therefore, the question becomes whether it is possible for a computer to analyze synoptic maps instead of people. If so, TC precipitation can be captured not only reliably, but also quickly and objectively.

Based on such a consideration, a numerical technique for estimating TC precipitation, which is named as the Originally Objective Method (OOM), was developed by Ren et al. (2001). This technique overcomes the disadvantages mentioned above. However, the method was first developed for a relatively complete analysis for Atlantic Ocean hurricanes influencing U. S. A. and only a few case studies for the WNP basin. The characteristics of the TC size varies regionally and TC sizes in the WNP TCs are characteristically larger than those in its Atlantic counterparts (Merrill, 1984; Liu and Chan, 1999). The technique need to be further tested before it can be applied to TCs in the WNP basin, which is the objective of this study.

In this study, in order to improve the technique for China, a comparison analysis between the objective method and ESM was carried out, and then, an advanced technique, which is called Objective Synoptic Analysis Technique (OSAT) for partitioning TC pre-

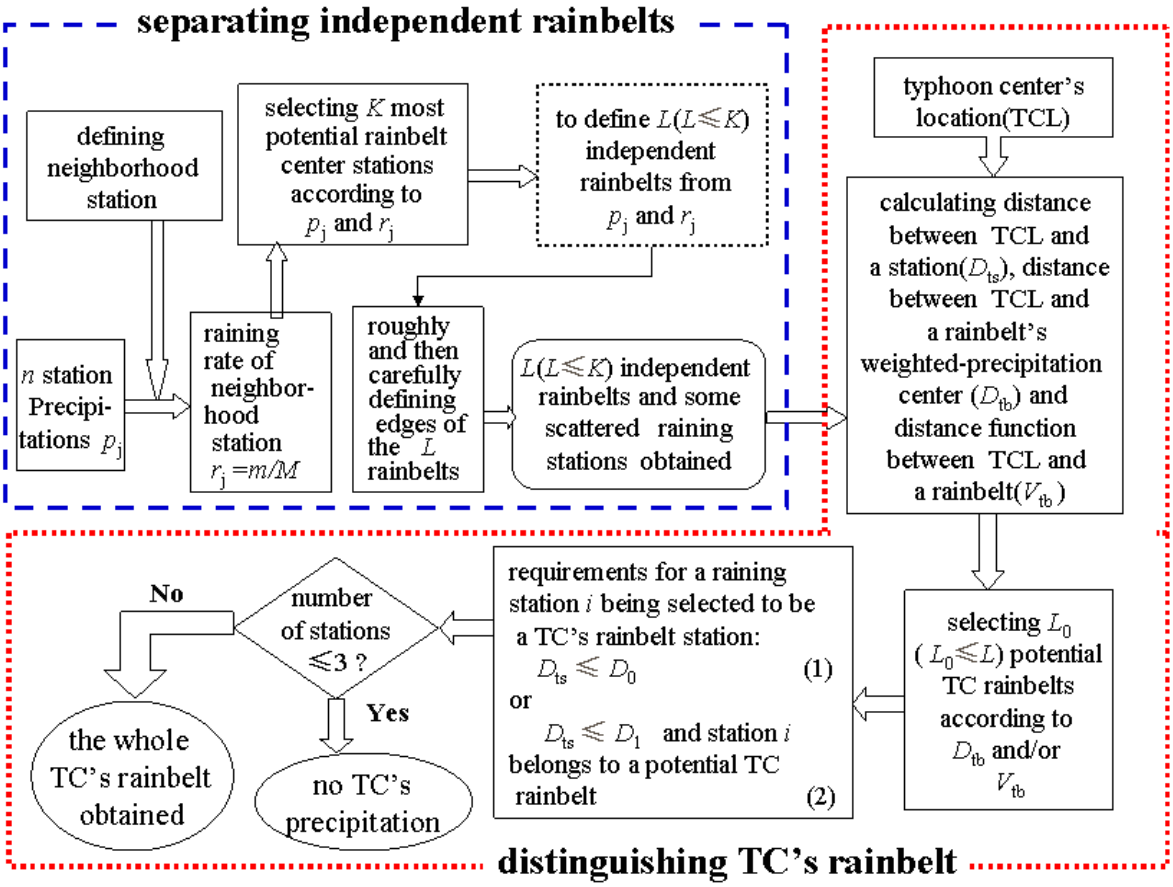

Fig. 2. A flowchart of the Objective Synoptic Analysis Technique (OSAT) for partitioning TC precipitation in China.

cipitation and briefly described by Wang et al. (2006), has been obtained.

2. The advanced technique

TC precipitation can result from the TC eyewall and spiral rainbands, or from the interactions between the TC circulation and other local weather systems. Two parameters are used to define the size of a TC, referred to as D in this study: D_1 and D_0, which are the maximum and minimum values, respectively. There may also be several independent rainbelts, which are generally asymmetric with respect to a TC center, and some scattered precipitation stations within D at a given time.

The idea behind OSAT is to imitate the process by which a weather forecaster manually analyzes a synoptic map. Suppose on a daily surface weather map, the precipitation distribution and position of a TC center are labeled. To analyze the TC precipitation, a weather forecaster usually takes two steps: first, based on the structure of the precipitation distribution, the daily precipitation field is separated into several independent rainbelts and some scattered precipitation stations and second, according to the forcaster's experience and the relationship between the TC center and the independent rainbelts and scattered precipitation stations, the weather forecaster can visually determine which rainbelts are associated with a given TC.

Here, we let the daily precipitation be denoted as $p(1), p(2), \cdots, p(n)$, for the stations that are located at longitudes of lon(1), lon(2), $\cdots$, lon(n) and latitudes of lat(1), lat(2), $\cdots$, lat(n) (Fig. 1a). In this example, a TC center is located over the delta of the Yangtze River, as shown in Fig. 1b. As a weather forecaster will do to Fig. 1, OSAT also takes two steps: first separating independent rainbelts from one another and then distinguishing the TC rainbelts. Figure 2 presents the fowchart of the OSAT and a detailed procedure is provided in the following section.

2.1 *Separating the independent rainbelts*

2.1.1 *Computing raining rate of neighborhood stations*

First, for given station j ($j = 1, 2, \cdots, n$), neighborhood stations may be defined as those stations that

are located within a certain distance (such as 200 km). For the raining station j ($p(j) > 0$), the raining rate of the neighborhood stations is

$$r(j) = m/M, \quad j = 1, \ldots, n \tag{1}$$

where M and m are the number of neighborhood stations and the raining neighborhood stations, respectively. The value of $r(j)$ ranges from 0.0 to 1.0 with a station with no precipitation ($p(j) = 0$), having $r(j)$ set to 0.

2.1.2 *Selecting the most potential rainbelt centers*

For station j, when $r(j)$ is greater than a certain value R_0, it belongs to a certain rainbelt. So there are three steps. First, it is necessary to sort the values of $r(j)$, for each of the n stations, in descending order. Second, the station with the largest raining rate of the neighborhood stations is selected as a most potential rainbelt center (simply called rainbelt center from now on). Finally, other $n-1$ stations are checked as well, and in this step, each of the $n-1$ stations can be selected as a most potential rainbelt center if the following requirements are all satisfied,

$$r(j) > R_0 \tag{2}$$

and

$$d > d_c \tag{3}$$

where d is the minimum distance between station j and any other rainbelt center that has already been defined, and d_c is a constant, predefined distance (such as 300 km). In order to separate all of the independent rainbelts from one another, R_0 is generally set to $0.3 - 0.5$.

2.1.3 *Defining the main characteristics of a rainbelt*

Now if we suppose that K rainbelt centers have been defined, for each of the K rainbelt center stations, the following procedure must be carried out.

Step 1: If the station doesn't belong to any particular rainbelt, it is said to belong to a new rainbelt l.

Step 2: If station j belongs to rainbelt l, for any of its neighbor stations, and it does not belong to any other rainbelts, it belongs to rainbelt l if either of the following two conditions is met:

$$p(j) \geqslant P_0 \quad \text{and} \quad r(j) \geqslant R_0\,, \tag{4}$$

$$p(j) > 0 \quad \text{and} \quad r(j) \geqslant 0.5\,. \tag{5}$$

In order to separate the rainbelts that are connected together by small precipitation, (4) and (5) are required for large and small precipitation, respectively. Here, P_0 is the threshold for separating large and small precipitations (empirically 5 mm). For example, in Fig. 1b the rainbelts indicated by "▲" and "●" are independent. As the potential bridge station "●", which is the closest one to rainbelt "▲", had a small precipitation ($p(j) < 5$ mm) with $r(j) < 0.5$, it cannot be considered a real "bridge" connecting the two independent rainbelts "▲" and "●".

Step 3: For a station that is selected as a member of rainbelt l, step 2 is repeated until there are no neighbor stations that match these requirements. Once this is completed, we return to step 1 for the next rainbelt center station to be analyzed.

2.1.4 *Roughly defining edges of the L rainbelts*

Now suppose that L ($L \leqslant K$) rainbelts have been defined through the above procedure. The following step only deals with the scattered raining stations ($p(j) > 0$) that don't belong to any rainbelt after the steps in the preceding section were completed. For each of these stations the following process is established:

Step 1: Among its neighbor stations, the numbers of stations that belong to the L different rainbelts are counted as numbers (1), (2), …, (L).

Step 2: For a maximum number ($l_{\max}$), only when $l_{\max} > 0$, the station belongs to rainbelt $l_{\max}$, otherwise it is considered a scattered raining station.

2.1.5 *Carefully defining edges of the L rainbelts*

After obtaining a rough definition of the edges of the L rainbelts, procedure 2.1.4 may be repeated one or more times to define the edges of the L rainbelts more accurately.

As of this stage in the process, L independent rainbelts (Fig. 1b) and some scattered raining stations (Fig. 1b, identified by "○") have been successfully separated.

2.2 *Distinguishing TC rainbelts*

TCs can influence China by both landfall and a passby. If the minimum of the distance between the TC center and a station (any of the n stations) is $D_{\min}$ ($D_{\min} \approx 0$ when landfall or on the land), the TC precipitation can be effectively distinguished as defined in the upcoming section.

2.2.1 *Selecting potential TC rainbelts*

A potential TC rainbelt may be defined when either of the following two requirements is met:

$$D_{\rm tb} < D_0 + D_{\min}\,, \tag{6}$$

$$\sum v(k) \geqslant 8.0, \;\; k = 1, \ldots, M_l\,, \tag{7}$$

where

$$v(k) = \begin{cases} 4.0 & \text{where } d(k) \leqslant 300 \text{ km} + D_{\min} \\ 2.0 & \text{where } 300 \text{ km} + D_{\min} < d(k) \leqslant 400 \text{ km} + D_{\min} \\ 1.0 & \text{where } 400 \text{ km} + D_{\min} < d(k) \leqslant 500 \text{ km} + D_{\min} \\ 0.5 & \text{where } 500 \text{ km} + D_{\min} < d(k) \leqslant 600 \text{ km} + D_{\min} \\ 0.0 & \text{else .} \end{cases}$$

Here, $D_{\rm tb}$ is the distance between the TC center and the rainbelt-weighted-precipitation center, M_l is the number of stations that rainbelt l possesses, and $v(k)$ is a function of the distance $d(k)$ between the TC center and station k of rainbelt l.

For example in Fig. 1b, there is only one potential TC rainbelt, which includes both the TC rainbelt "•" and the rainbelt that is located in the center-northern portion of Northeast China.

2.2.2 *Defining the whole TC rainbelt*

For a certain raining station j, it belongs to the whole TC rainbelt when either of the following two requirements is met:

$$D_{\rm ts} < D_0 \tag{8}$$

$$D_{\rm ts} < D_1 \quad \text{and station } j \text{ belongs to a potential TC rainbelt ,} \tag{9}$$

where $D_{\rm ts}$ is the distance between the TC center and station j, and D_0 and D_1 are generally referred to as the thresholds for the distance of the absolute TC precipitation and for TC size (radius), respectively. In some cases, a potential TC rainbelt is produced by the interactions between a TC and other local weather systems, in this case D_1 is used to distinguish TC precipitation from that of other systems. After this process, the whole TC rainbelt (Fig. 1b, identified by "•") can be defined. In addition, if the number of stations belonging to the TC rainbelt is not greater than three, no value for the TC precipitation can be estimated.

In WNP, the typical values of D_0 and D_1 are 500 km, which is the maximum of the distance between a TC center and its squall in front of it, and 1100 km, which is usually given as the maximum of the radius for a TC's outlet (Brand, 1972; Elsberry et al., 1987), respectively. In this technique, D_0 and D_1 are variable parameters according to TC's intensity (maximum wind speed) (Table 1).

3. Description of data and comparison analysis

The WNP TC data used in this study were supplied by the Shanghai Typhoon Institute, which contain 6 hourly positions, estimated maximum sustained wind speed (MSWS) and MSLP of each TC occurrence during the period between 1949 and 2005. Two daily precipitation datasets are available in this study. One includes data collected from 677 Chinese stations, in which 659 stations were from the National Meteorological Information Center and the other 18 were from Taiwan Island. The other was a daily TC precipitation dataset acquired by the Shanghai Typhoon Institute (also referred to as the ESM dataset later in this article), which was composed of 1474 stations. Figures 3a and 3b show the distribution of the 677 stations and that of 1474 stations from these two datasets, respectively. A close inspection of the two datasets reveals that the time coverage of the daily precipitation for the 659 stations was from 0000 UTC to 2400 UTC. The station numbers continue to increase during the period between 1951–2000, with a sharp rise from about 170 in 1951 to approximately 610 in 1959. Meanwhile, the time coverage of the daily TC precipitation for the 1474 stations varied in the past, from 0000 UTC to 2400 UTC during the period from 1949 to 1984 and from 2000 UTC the previous day for a full 24 hour period for the timeframe between 1985 and 2003. In addition, the daily TC precipitation data was discontinuous for most stations over the past 55 years.

Considering the uncertainties involved in the different datasets, the period 1951–2003 was selected for the comparative analysis. A TC was defined as an influencing TC only when it produced a rainbelt over the mainland of China or any of the two biggest islands of China, Taiwan and Hainan. Thus, influencing TCs include both those TCs that made landfall and those that passed just offshore of the Chinese mainland.

In order to verify the OSAT's capability for partitioning the TC precipitation, daily station precipitation data from all over China during 2005 and NOAA's CMORPH (Climate Prediction Center MORPHing technique) daily precipitation were applied to this study. At present, CMORPH precipitation data is the combined estimates that are derived from the passive microwaves aboard the U. S. Air Force Defense Meteorological Satellite Program (DMSP) satellites 13, 14 and 15 (SSM/I), the NOAA-15, 16 and 17 (the Advanced Microwave Sounding Units B, AMSU-B) and the Tropical Rainfall Measuring Mission (TRMM)(TMI) spacecrafts. CMORPH produces global precipitation analyses with very high spatial (0.07277 degrees lat/lon, 8 km at the equator) and

Table 1. Values of D_0 and D_1 as a function of the TC maximum wind speed

	TC's maximum sustained wind speed (Unit: m s^{-1})	D_0 (Unit: km)	D_1 (Unit: km)
TCs far away from China	$u < 17.2$ (tropical depreesion)	200	600
($D_{\min} > 300$ km)	$17.2 \leqslant u < 24.4$ (tropical strom)	300	800
	$24.4 \leqslant u < 32.6$ (strong tropical strorm)	400	1000
	$u \geqslant 32.6$ (typhoon and above)	500	1100
TCs close to China	$u < 17.2$ (tropical depression)	300	800
($D_{\min} \leqslant 300$ km)	$u \geqslant 17.2$ (tropical strom and above)	500	1100

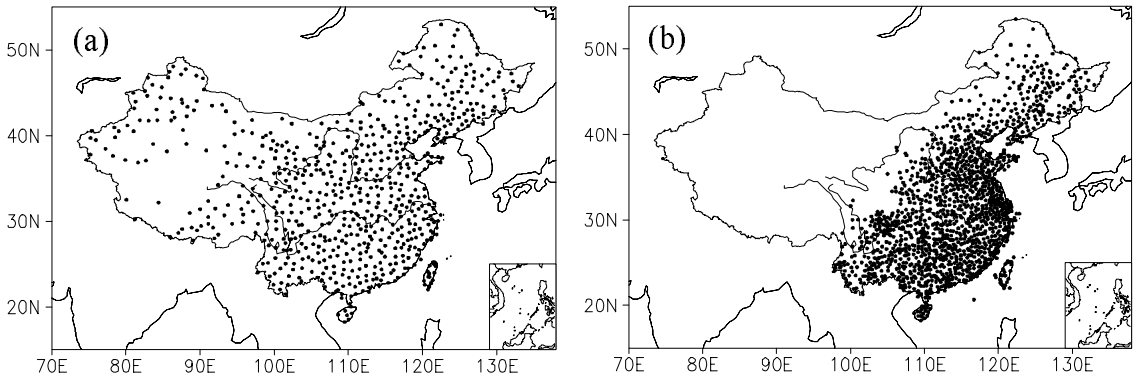

Fig. 3. The distributions of the two datasets from the stations, (a) the 677 stations and (b) the 1474 stations as discussed in the text.

temporal (30 minutes) resolution and the period of record for the CMORPH daily precipitation dataset was from 3 December 2002 to the present.

In the comparison analysis, the differences between the results obtained by the objective method and the ESM were mainly due to the differences in the coverage associated with the two different techniques.

A diagram of the TC precipitations obtained via the objective method (A) and the ESM (B) are presented in Fig. 4. The common area is defined as $\mathrm{A} \cap \mathrm{B}$ and the total area is $\mathrm{A} \cup \mathrm{B}$. Two difference indices were used and are defined as follows:

$$Q = (A \cup B) - (A \cap B)\,, \tag{10}$$

$$P = (A \cap B)/(A \cup B)\,, \tag{11}$$

where Q is absolute difference in the area between the two methods, with a larger Q implying that the difference is more significant. Meanwhile, P is defined as the area consistent rate between the two methods, with the values ranging from 0 to 1, where a smaller P means that the difference is more significant. When $Q \to 0$ and $P \to 1$, results from the two methods are approximately the same. In other words, if the result of ESM is ideal, then the data obtained by the objective method is as well.

In this study, a $0.5^\circ \times 0.5^\circ$ latitude-longitude grid was used. Inverse-distance interpolation was applied to transform the TC rainband station data onto the aforementioned grid mesh. To limit the TC rainband expansion, this grid procedure was confined to the region where the TC rainband was distributed. As a grid can also represent a quadrangle, it was easy to calculate the area represented by a given grid as,

$$A_{\mathrm{grid}} = (\pi r/360)^2 \times \cos\varphi\,, \tag{12}$$

where r is the radius of the Earth, φ is the latitude of the grid, and A_{grid} was the grid area in km^2. The values of A_{grid} are summed over the TC rainbelt grids to yield the size of the impacted area as follows:

$$A = \sum_{k_1=1}^{l_1} A_{k_1}, \quad B = \sum_{k_2=1}^{l_2} B_{k_2}\,, \tag{13}$$

where l_1 and l_2 are the numbers of grids comprising the two TC rainbelts.

Based on these two indices, three different indices were defined:

Daily indices: For a certain day, two indices can be defined as

$$Q_{\mathrm{d}} = Q\,, \tag{14}$$

$$P_{\mathrm{d}} = P\,, \tag{15}$$

where Q_{d} and P_{d} are called the daily-absolute-area difference and daily-area-consistent rate, respectively.

Case indices: For a certain TC case, two indices

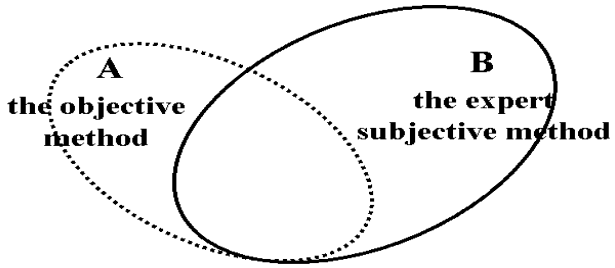

Fig. 4. A Sketch map for the TC precipitations from the objective method and the expert subjective method.

can be defined as

$$Q_{\rm g} = \sum_{i=1}^{n} Q_{di} \ , \tag{16}$$

$$P_{\rm g} = \frac{\sum\limits_{i=1}^{n}(A_i \cap B_i)}{\sum\limits_{i=1}^{n}(A_i \cup B_i)} \ , \tag{17}$$

where $Q_{\rm g}$ and $P_{\rm g}$ are the case-accumulated-absolute-area difference and case-accumulated-area-consistent rate, respectively, and n is the number of days when a TC was found to influence China.

Overall indices: For a certain period, such as a year or longer, two indices can be defined as

$$Q_{\rm t} = \sum_{j=1}^{m}\sum_{i=1}^{n_j} Q_{dij} \ , \tag{18}$$

$$P_{\rm t} = \frac{\sum\limits_{j=1}^{m}\sum\limits_{i=1}^{n_j}(A_{ij} \cap B_{ij})}{\sum\limits_{j=1}^{m}\sum\limits_{i=1}^{n_j}(A_{ij} \cup B_{ij})} \ , \tag{19}$$

where $Q_{\rm t}$ and $P_{\rm t}$ are the overall-accumulated-absolute-area difference and overall-accumulated-area-consistent rate, respectively, while m and n are the number of TC cases occurring during the period and the number of days for case j, respectively.

4. Results and discussions

Figure 5 depicts the $Q_{\rm g} - P_{\rm g}$ distribution for the TC cases of OOM. Totally, there are 1811 TC cases that occurred during 1951–2003 and OOM identified 1013 cases that influenced China. The indices showed that the differences between OOM and ESB were relative large, with average $Q_{\rm g}$, maximum $Q_{\rm g}$ and average $P_{\rm g}$ being 1.26×10^6 km^2, 7.79×10^6 km^2 and 0.29, respectively. Further inspection revealed that significant differences between OOM and ESM may be sorted as three different types:

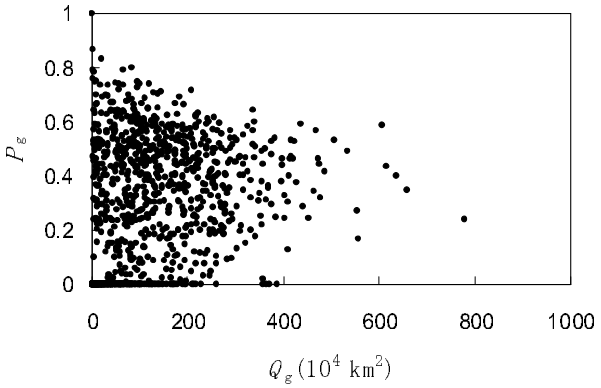

Fig. 5. $Q_{\rm g} - P_{\rm g}$ distributions for some TC cases from OOM.

(1) $P_{\rm g} = 0, Q_{\rm g} > 0$ ($\sum\limits_{i=1}^{n} A_i = 0, \ \sum\limits_{i=1}^{n} B_i > 0$); the case where ESM recognized the TC precipitation while OOM did not. This type had 9 cases and $Q_{\rm g}$ was very small, with values ranging between 5×10^3 km^2 and 1.4×10^5 km^2. The situation involving this type was that ESM recognized the TC precipitation, the area of which was very small, along the coast or parts of the two islands. The difference results from the different methods of dealing with the small-area TC precipitation.

(2) $P_{\rm g} = 0, \ Q_{\rm g} > 0$ ($\sum\limits_{i=1}^{n} A_i > 0, \ \sum\limits_{i=1}^{n} B_i = 0$); namely the case where the OOM recognized the TC precipitation and the ESM did not. There were 264 cases of this type, with 115 cases having a $Q_{\rm g}$ less than 2×10^5 km^2, 109 having $Q_{\rm g}$ falling between 2×10^5 km^2 and 1×10^6 km^2, and the last 40 cases having $Q_{\rm g}$ falling between 1×10^6 km^2 and 2.87×10^6 km^2. Further examination reveals that there were two reasons for this type to occur, (a) for cases with small $Q_{\rm g}$, OOM recognized the TC precipitation (more than 3 stations) along the coast or parts of the two islands while the ESM did not or (b) some TC precipitation data was lacking or the wrong dates were used for some of the TC cases in the ESM dataset. Some examples include the 17th case that occurred in 1961, the 49th case of 1967 and the 15th case of 1984.

(3) $P_{\rm g} \neq 0$; with a very small $P_{\rm g}$ and a large $Q_{\rm g}$, In this case, the case-accumulated-area-consistent rate was small, while the case-accumulated-absolute-area difference was large. After a careful inspection, three reasons for this type were determined as follows:

(a) Some important parameters of the OOM needed to be adjusted. For instance a large $Q_{\rm g}$ is due to large $Q_{\rm d}$. In order to analyze the possible relationships between the different indices and the TC intensity, a statistical analysis of the TC intensity for the days with the most significant difference yields

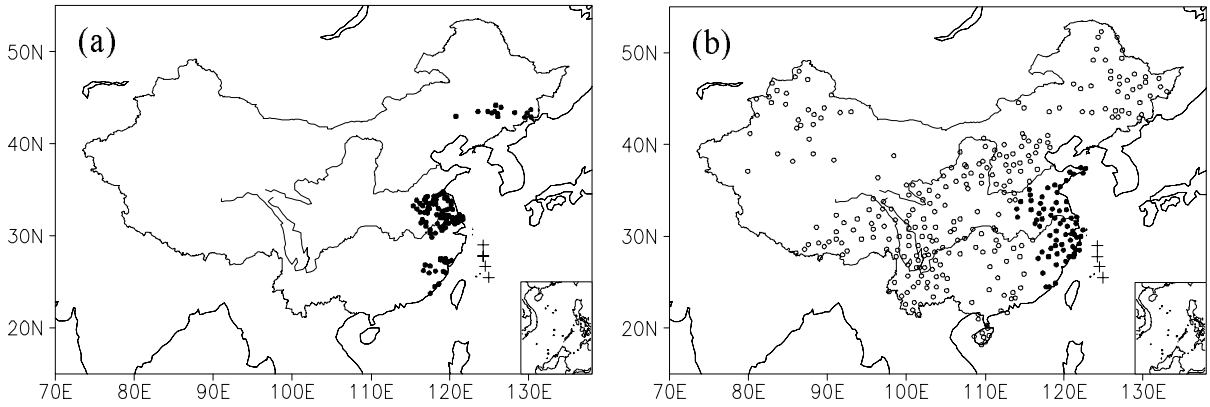

Fig. 6. The results of the partitioning of the TC rainbelt using (a) ESM and (b) OOM for the data from 4 July 2002 in China. The "+" denotes the location of the TC center, the "•" symbol denote the TC precipitation, and the "○" symbol represents the precipitation due to the other local weather systems.

$0.38 > P_d > 0$ and $Q_d > 1.5 \times 10^6$ km^2.

Statistical results show that for the 15 days with the most significant differences, the TC's MSWSs were all smaller than 12.1 m s^{-1}. In other words, the 15 days with the most significant differences occurred during tropical depressions (when MSWS<17.2 m s^{-1}). Comparison analysis with synoptic "hand-analysis" maps revealed that this was due to an unreasonable expansion of the TC precipitation area by OOM. In OOM, it is one of the main reasons that the parameters D_0 and D_1, which are 500 km and 1100 km, respectively, are fixed, with no consideration of the relationship between these parameters and the TC intensity. It should be expected that these 15 cases would be improved if D_0 and D_1 were smaller.

(b) The time coverage of the daily data from the two datasets were very different from each other (see section 3 for details).

(c) There were some potential errors in the ESM dataset.

The 7th TC Rammasun in 2002 influenced China significantly. Figure 6 presents the results of partitioning the TC precipitation using both ESM and OOM for the data of 4 July 2002. The TC rainbelt distributions that resulted from OOM are more reasonable than those resulting from ESM, as the rainbelt in Northeast China, which was more than 1500 km away from TC center, shouldn't be considered as a TC precipitation. Inspection of weather maps also showed that there was a cold front with a depression in Northeast China during 4–5 July 2002.

Based on the above comparison analysis, it was revealed that defining D_0 and D_1 as fixed parameters was the main problem for OOM. Therefore, it is necessary to allow these to be considered as variables. Furthermore, considering that the interactions between TCs and middle latitude systems tend to result in more frequent far-distance heavy rainfall after or around the time of a TC's landfall, these parameters need to be variable and their values should be determined according to the relative distance between the TC and the mainland of China. The principle for designing the developing scheme of OOM was defined as follows: (1) Values of these parameters vary according to TC categories, with small values being used for low-level grades, where the value ranges for D_0 and D_1 are defined as [200 km, 500 km] and [500 km, 1100 km], respectively. (2) The values of D_0 and D_1 for TCs that are close to China should not be smaller than those for TCs far from China.

Under these conditions, 12 different schemes (including OOM itself) were designed and the $Q_t - P_t$ distributions for these schemes are presented in Figure 7. Obviously, the worst one is OOM, which had the maximum value of $Q_t(1.39 \times 10^9$ km$^2)$ and the mini-

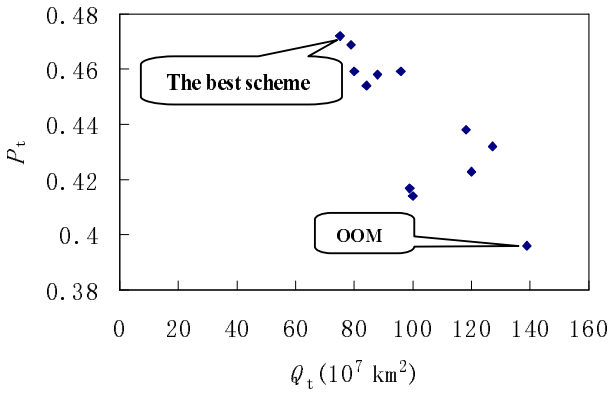

Fig. 7. The $Q_t - P_t$ distribution for the 12 developing schemes as discussed in the text.

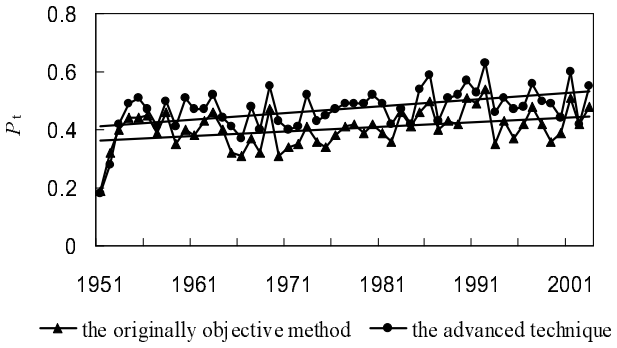

Fig. 8. Variations in the annual, accumulated-areas-consistent rates between OOM (or OSAT) and ESM.

mum value of $P_t(0.396)$ for any of the 12 schemes. Meanwhile, OSAT was the best, which was introduced in detail in section 2, with the minimum value of $Q_t(7.5\times10^8$ km$^2)$ and the maximum value of $P_t(0.472)$ for any of the 12 schemes being observed.

Two conclusions can be reached through the comparison of the performance of both OOM and OSAT:

(1) OSAT is much better than OOM. Figure 8 shows that the annual P_t of OSAT is greater than that of OOM for every year since 1953 and for the period between 1951–2003, the average P_t showed an increase of 0.07. For the extreme situation, OSAT's maximum Q_g and Q_d were 4.88×10^6 km^2 and 1.78×10^6 km^2, which are significantly smaller than the values of 7.79×10^6 km^2 and 2.40×10^6 km^2 that were obtained for OOM, respectively. In addition, the averages of Q_g and Q_d for OSAT were 9.4×10^5 km^2 and 2.3×10^5 km^2, which were both smaller than the values of 1.26×10^6 km^2 and 2.9×10^5 km^2 obtained for OOM, respectively. (2) The effect of an objective method on the final results was quite sensitive to the number of stations, especially when that number was less than 400. However, when the number was greater than 400, the results obtained via an objective method were relatively stable with only a slightly increasing trend with the number of stations.

Figure 9 presents the results from the partitioning of the TC precipitation in China for TCs Koni and Imbudo using OSAT. Koni's lifetime was from 15 to 23 July 2003, while Imbudo's lifetime encompassed the time between 16 and 25 July 2003. Both of these TCs influenced China from 22 to 23 July. On 22 July, Koni crossed the Beibu Gulf and produced precipitation over western South China and southern Southwest China, while Imbudo passed North Philippine and only brought the TC edge precipitation along the eastern coast of Guangdong. On the next day, precipitations from the remnants of Koni covered southern Yunnan and southwestern Guizhou, while Imbudo's rainbelt occurred in Hainan and Guangdong. After comparison with the CMORPH precipitation data, these results proved to be reasonable. In other words, OSAT has the capability to distinguish precipitation rainbelts for different TCs at the same moment quite well.

Matsa was the most serious TC case that influenced China in 2005. Figure 10 depicts the precipitation distribution and the TC rainbelt using OSAT during the period from 3 to 9 (for brevity, some figures are not shown) August 2005.

It is necessary to describe the large-scale pattern. At 500 hPa geopotential height fields on 3 August 2005, the WNP high was very strong and extended westward over southeastern China, while a strong trough covered the Chinese mainland from the North to the Southwest, including a cyclone over southern North China. As the WNP high was stable and blocked the trough from moving directly eastward, the trough was maintained from 4 to 6 August, and weakened slowly, with its southern part merging into Matsa and its northern part continuing northeastward along the northwestern edge of the WNP high. In the 850 hPa geopotential height and wind fields, a strong shear line was observed over the mainland of China and its variations were similar to the 500 hPa trough observed during the same period.

On 6 August, TC Matsa made landfall at Zhejiang Province and under the leading air flow it continued northwestward and then eventually northward across East China (Fig. 10d), while the inverse trough of Matsa interacted with the shear line during the period between 4 and 6 August.

Figures 10a–c show daily station precipitation distributions and the TC rainbelts. Between 4 to 9 August 2005, there was always a large precipitation area located in eastern China, which during the first 3 days was mainly produced through the interactions between Matsa and the wind shear and during the next 3 days resulted mainly from the interactions between the Matsa circulation and a new, small, westerly trough moving in from the west. In order to verify the TC rainbelt, NOAA's CMORPH precipitation maps are provided as Figs. 10e–g. On 3 August, CMORPH map show that Matsa produced rainfall only over Taiwan Island, and on the next day, the CMORPH precipitation and circulation (wind data) show the southeast coast being impacted by Matsa. On 5 August, Matsa influenced most of East China and on the next day its rainbelt extended northwestward, into eastern Center China. On 7 August, Matsa moved northward and its impact reached northern Center China and southern North China and on 8 August, Matsa was observed to have moved northward quickly and had begun to influence the Northeast. By 9 August, Matsa had weak-

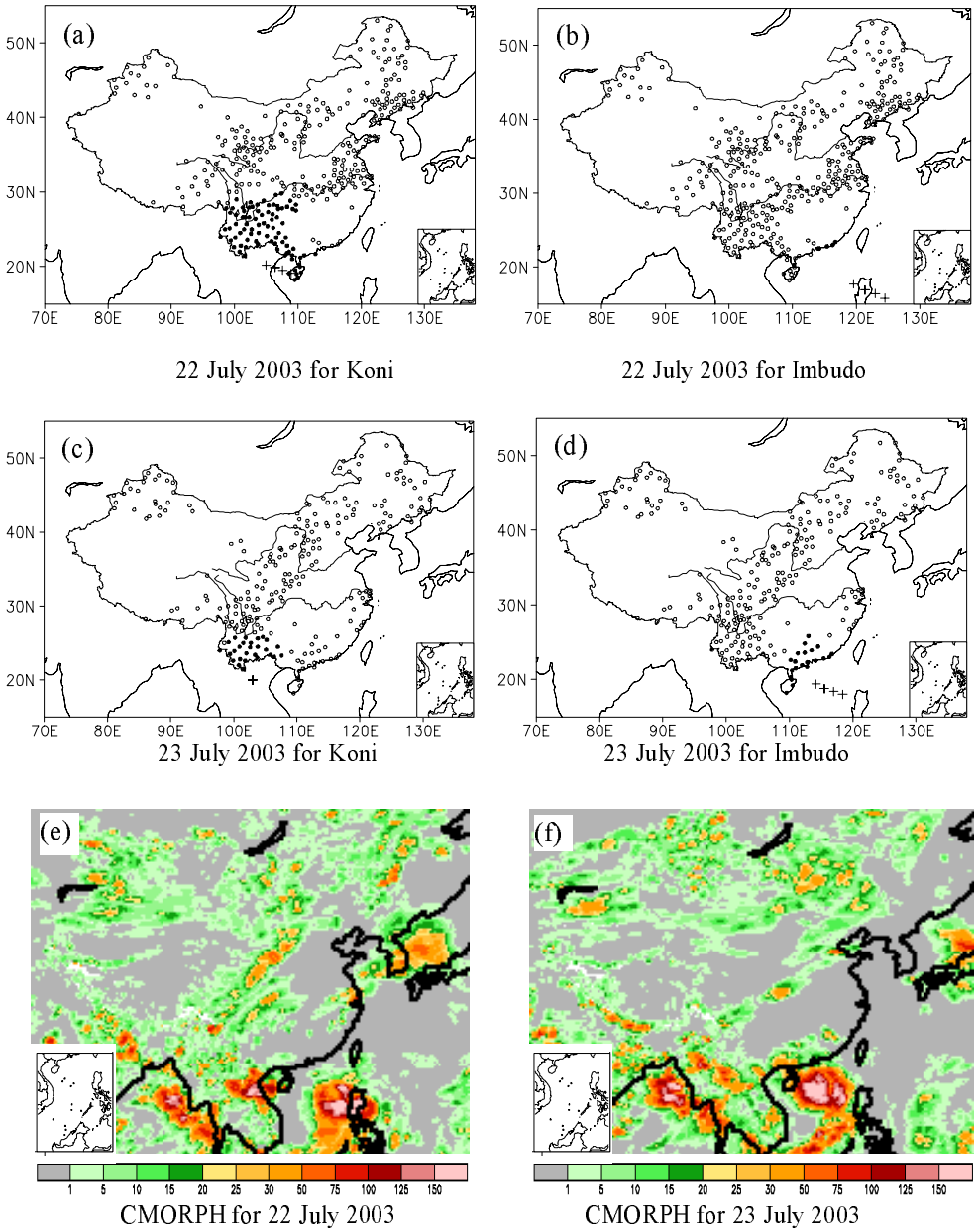

Fig. 9. (a)–(d) Results of the partitioning of the TC precipitation in China for two TCs, Koni and Imbudo, during a given day using OSAT. The "+" denotes the location of the TC center, the "•" symbol represents the TC precipitation and the "○" symbol represents the precipitation due to other local weather systems. (e)–(f) The associated CMORPH precipitation maps.

ened quickly and its precipitation was mainly observed in parts of the Northeast. Based on the above analysis and the absence of precipitation data for Taiwan Island, the TC rainbelts using OSAT for Matsa in Figs. 10a–c were relatively reasonable, and OSAT showed the capability to separate the TC precipitation from the inverse trough of Matsa that was created from a shear line. Figure 10d also shows that Matsa brought precipitation into a large area, about 1000 km away from its track.

5. Summary

An advanced technique for estimating TC precipitation from station observations, named OSAT, has been developed. Some conclusions can be drawn as follows:

(1) Comparison analysis between OOM and ESM

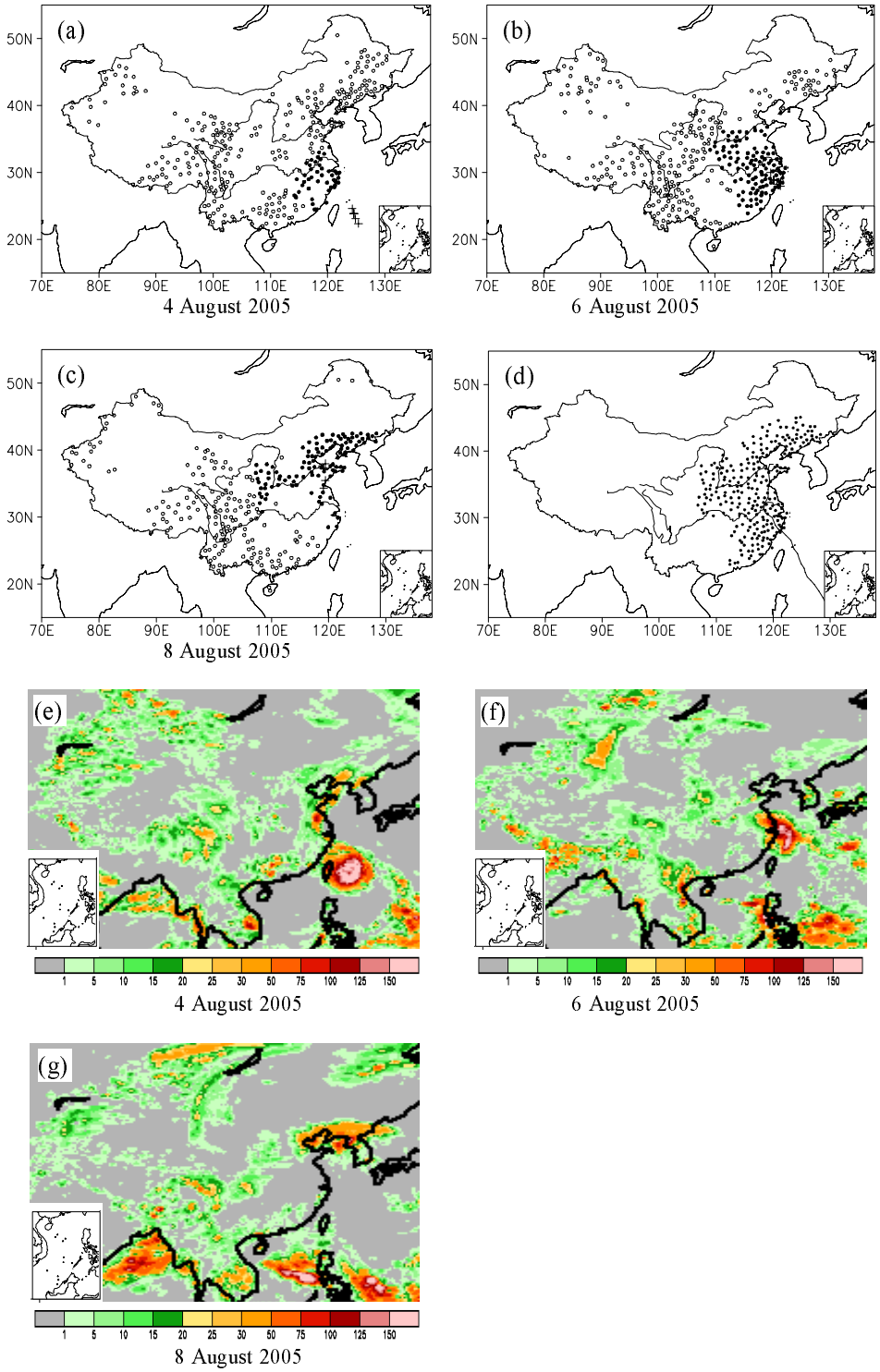

Fig. 10. The precipitation distributions and TC rainbelt using OSAT during the period of from 3 to 9 August 2005 showing TC Matsa influencing China. (a)–(c) present the daily station precipitation distributions and the TC rainbelts using OSAT, while (e)–(g) present NOAA's CMORPH daily precipitation distributions. TC Matsa's track and distribution of stations that were influenced by Matsa are presented in (d). In Fig.10 (a)–(d), "•" represents the TC precipitation, while "o" represents the precipitation due to other weather systems (rainfall data for the Taiwan Island was not available). The "o" denotes the location of the TC center and the solid line represents the path of the TC.

revealed that for partitioning TC precipitation in China, the main problem with OOM was that the thresholds for the distance of the absolute TC precipitation (D_0) and the TC size (D_1) were fixed, while it was observed that more accurate results could be obtained if these parameters were allowed to vary.

(2) Results of OSAT showed significant improvements in the simulation of the overall-accumulated-absolute-area difference, Q_t, the accumulated-area-consistent rate, P_t, the extreme and average daily indices (Q_d and P_d, respectively) and the case indices (Q_g and P_g, respectively).

(3) This case study indicates that OSAT showed the capability to distinguish precipitation rainbelts for different TCs from those associated with middle-latitude weather systems.

Actually, the difference between the results acquired by OSAT and those from ESM are still significant. The above comparitive analysis suggests that there may be two main reasons for this: (1) the differences between the two datasets, especially the difference in the date-time coverage and (2) some yet unknown shortcomings may still exist in either OSAT or ESM, which may also result in the observed differences between the results.

In conclusion, OSAT has shown significant improvements when compared with OOM and has been presented as being quite capable in partitioning the TC's precipitation. It can be expected that this progress may enhance the basis for the study of TC precipitation climatology and TC disaster assessment.

Acknowledgements. The authors would like to express their sincere thanks to Prof. Wu Guoxiong, Dr. Wu Liguang, Prof. Dong Wenjie, Dr. Zhang Peiqun, Dr. Lei Xiaotu and Mr. Muhammad Afzaal for their helpful suggestions and discussions concerning this study. This work was supported by the Chinese Ministry of Science and Technology Project (Grant No. 2006CB403601) and the Special Foundation of Shanghai Typhoon Institute, China Meteorological Administration under the 2005 project.

REFERENCES

Akira, H., 2005: Tropical cyclone and heavy precipitation over the western north pacific in present and Doubled CO_2 climates simulated by the CCSR/NIES/FRCGC T106 AGCM. *The 2nd International Workshop on the Kyosei Project*, 24–26 February, Hawaii.

Brand, S., 1972: Very large and very small TC of the western North Pacific Ocean. *J. Meteor. Soc. Japan*, **50**(4), 332–341.

Elsberry, R. L., W. M. Frank, G. J. Holland, J. D. Jarrell and R. L. Southern, 1987: *A Global View of Tropical Cyclones*. University of Chicago Press, 185pp.

Gleason, B. E., D. R. Easterling, and F. Ren, 2000: Trends in tropical cyclone precipitation over the eastern United States. *Preprints, 12th Conf. on Applied Climatology*, Asheville, NC., Amer. Meteor. Soc., 320–323.

Liu, K. S., and J. Chan, 1999: Size of tropical cyclones as Inferred from ERS-1 and ERS-2 data. *Mon. Wea. Rev.*, **127**, 2992–3001.

Merrill, R. T., 1984: A Comparison of large and small tropical cyclones. *Mon. Wea. Rev.*, **112**, 1408–1418.

Phil, J. E., and A. V. Douglas, 2001: The role of eastern North Pacific tropical storms in the rainfall climatology of western Mexico. *International Journal of Climatology*, **21**(11), 1357–1370.

Ren, F. M., B. Gleason and D. R. Easterling, 2001: A technique for partitioning tropical cyclone precipitation. *Journal of Tropical Meteorology*, **17**(3), 308–313. (in Chinese)

Ren, F. M., B. Gleason, and D. R. Easterling, 2002: TC Impacts on China's Precipitation During 1957–1996. *Adv. Atmos. Sci.*, **19**(5), 943–952.

Wang, Y., F. Ren, X. Wang, W. Li, and D. Shao, 2006: Development study on the technique for partitioning tropical cyclone precipitation in China. *Meteorological Monthly*, **32**(3), 6–10. (in Chinese)

Weatherford, C. L., and W. M. Gray, 1988a: TC structure as revealed by aircraft reconnaissance. Part I: Data analysis and climatology. *Mon. Wea. Rev.*, **116**, 1032–1043.

Weatherford, C. L. and W. M. Gray, 1988b: TC structure as revealed by aircraft reconnaissance. Part II: Structural variability. *Mon. Wea. Rev.*, **116**, 1044–1056.